

# IEEE Copyright Notice

Copyright (c) 2018 IEEE

Personal use of this material is permitted. Permission from IEEE must be obtained for all other uses, in any current or future media, including reprinting/republishing this material for advertising or promotional purposes, creating new collective works, for resale or redistribution to servers or lists, or reuse of any copyrighted component of this work in other works.

**Published in:** 2018 European Conference on Networks and Communications (EuCNC), 18-21 June, 2018, Ljubljana, Slovenia

**DOI:** 10.1109/EuCNC.2018.8443268

**Print at:** <https://ieeexplore.ieee.org/document/8443268>

**Cite as:**

Wheberth Dias, Danilo Garspar, Luciano Mendes, Marwa Chafii, Maximilian Matthé, Peter Neuhaus and Gerhard Fettweis, "Performance Analysis of a 5G Transceiver Implementation for Remote Areas Scenarios." 2018 European Conference on Networks and Communications (EuCNC). IEEE, 2018.

**BibTex:**

```
@inproceedings{dias2018performance,
  title={Performance Analysis of a 5G Transceiver Implementation for Remote Areas Scenarios},
  author={Wheberth Dias, Danilo Gaspar, Luciano Mendes, Marwa Chafii, Maximilian Matth{e}, Peter Neuhaus and Gerhard Fettweis },
  booktitle={2018 European Conference on Networks and Communications (EuCNC)},
  pages={363–367},
  year={2018},
  organization={IEEE}
}
```

# Performance Analysis of a 5G Transceiver Implementation for Remote Areas Scenarios

Wheberth Dias, Danilo Gaspar, Luciano Mendes, Marwa Chafii, Maximilian Matthé, Peter Neuhaus, Gerhard Fettweis

**Abstract**—Fifth generation of mobile communication networks will support a large set of new services and applications. One important use case is the remote area coverage for broadband Internet access. This use case has significant social and economical impact, since a considerable percentage of the global population living in low populated area does not have Internet access and the communication infrastructure in rural areas can be used to improve agrobusiness productivity. The aim of this paper is to analyze the performance of a 5G for Remote Areas transceiver, implemented on field programmable gate array based hardware for real-time processing. This transceiver employs the latest digital communication techniques, such as generalized frequency division multiplexing waveform combined with 2 by 2 multiple-input multiple-output diversity scheme and polar channel coding. The performance of the prototype is evaluated regarding its out-of-band emissions and bit error rate under AWGN channel.

**Index Terms**—PHY, 5G, GFDM, Polar Code, MIMO, Space-Time Coding, Remote Areas.

## I. INTRODUCTION

Fifth Generation (5G) Networks are being pointed as the next revolution in mobile communications [1], which will support several new services and applications. Several scientific and industrial efforts are currently being made in order to define the new radio interface for enhanced mobile broadband (eMBB), ultra-reliable low latency (URLL) and massive machine type communication (mMTC) applications [2].

However, one important scenario with huge social and economical impact is not being widely discussed by academia and industry: the 5G operation mode for remote areas. This scenario has very specific requirements and challenges [3]. Since the user density in rural areas is small, each base station (BS) shall cover a large area, leading to long channel delay profiles. Very High Frequency (VHF) and Ultra High Frequency (UHF) frequency bands can be exploited due to their good propagation properties. But, since these bands are also used for other services, i.e., digital television, 5G for remote areas physical layer (PHY) must employ a waveform with low out-of-band (OOB) emission, allowing for Cognitive Radio (CR) technologies and secondary network methodologies [4] to be employed. Also, the PHY must provide high

robustness against the channel impairments, using the state-of-the-art channel coding [5].

In [6], the authors propose a high spectrum efficient PHY based on multi user (MU)-multiple-input multiple-output (MIMO) for Orthogonal Frequency Division Multiplexing (OFDM) [7]. However, mechanisms that allow the coexistence with other legacy networks, reduce the OOB emissions and deal with large channel delay profiles are not considered. In [8], the authors present a medium access control layer (MAC)-PHY solution for supporting Internet of Things (IoT) and machine type communication (MTC) in rural areas, but without considering other important applications, such as broadband Internet access and latency sensitive services [9].

The aim of this paper is to evaluate the performance of a real-time implementation of a transceiver and frame structure, conceived to support 5G services in remote areas. The transceiver is based on a flexible novel modulation scheme, named Generalized Frequency Division Multiplexing (GFDM) [10]. GFDM can be tailored to efficiently use the cyclic prefix (CP) and cyclic suffix (CS) in severe multipath channels. It also presents very low OOB emissions and can be combined with MIMO techniques to provide robustness and spectrum efficiency [11] [12]. Polar encoder and decoder [13] [5] have also been implemented for real-time processing. In this paper, the bit error rate (BER) performance of single-input single-output (SISO) and MIMO GFDM system with polar channel coding under additive white Gaussian noise (AWGN) channel will be presented. The OOB emission will also be analyzed. In order to identify the impact of the hardware implementation into the system performance, two approaches are used for the measurements: i) noiseless channel estimation preambles, where noise is added only to the synchronization preamble and to the GFDM blocks and; ii) noisy channel estimation preambles, where noise is added to the entire GFDM frame. Theoretical and simulation BER curves are used as reference.

The remainder of this paper is organized as follows: Section II describes the real-time transceiver implementation, while Section III brings the systems performance analysis and Section IV concludes this paper.

## II. TRANSCEIVER DESCRIPTION

Figure 1 presents the block diagram of the proposed 5G transmitter and receiver. The 5G transceiver is able to operate in continuous data transfer mode (CDTM), where the time-frequency resource is continuously occupied, or in burst data transfer mode (BDTM), where the time-frequency resource is only allocated when there are useful data from users to be

Manuscript received February 22, 2018.

W. Dias, D. Gaspar and L. Mendes are with Inatel, Sta. Rita Sapucaí, Brazil. e-mail: {wheberth, danilo-gaspar, luciano}@inatel.br

M. Chafii, M. Matthé, P. Neuhaus and G. Fettweis are with TU Dresden, Dresden, Germany. e-mail: {first name.last name}@ifn.et.tu-dresden.de

This work was supported by CNPq-Brasil, Finep/CRR under Grant No. 01.14.0231.00 hosted by Inatel, and by 5G-RANGE Brazil-Europe joint project.

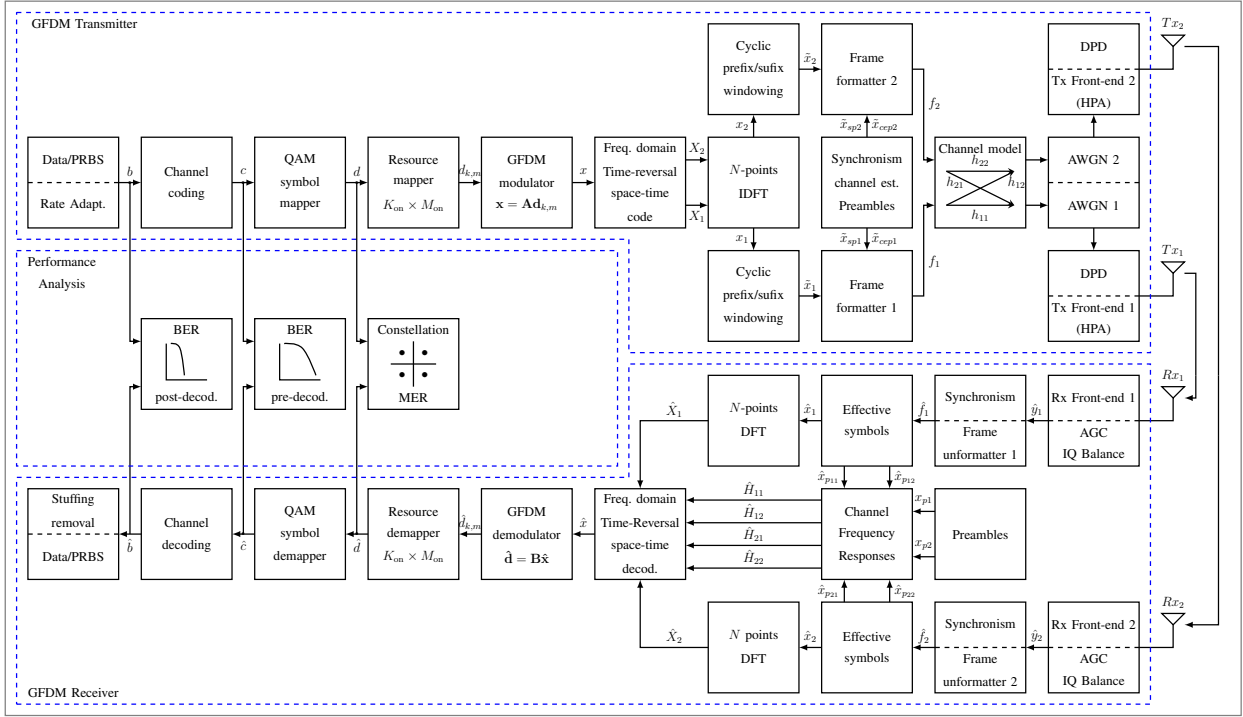


Fig. 1: Transceiver GFDM block diagram.

transmitted. Hereafter, a description of the main transceiver modules is provided.

On the transmitter side, a rate adaptation is performed through insertion of stuffing bits when the transceiver operates in CDTM and the income throughput is smaller than its capacity. An internal Pseudo Random Bit Sequence (PRBS) can be selected in order to allow system performance evaluation.

Next to rate adaptation, income data are encoded by the Channel Coding block, responsible for adding redundancy information to the sequence, seeking to improve the robustness of the system against impairments introduced by the channel. Polar code was chosen to compose the first transceiver version due to its low complexity and superior performance considering short code words [14]. Polar code is implemented under Successive Cancellation decoding (SCD), using the shortening technique described in [15] with selectable code rates of 1/2, 2/3, 3/4 and 5/6.

The encoded data sequence is mapped according to a quadrature amplitude modulation (QAM) constellation. The available configurations are 4-QAM, 16-QAM, 64-QAM or 256-QAM.

GFDM waveform can be seen as a time-frequency resource grid, arranged in  $K$  sub-carriers in frequency and  $M$  subsequent sub-symbols in time. Thereby, a total of  $N = KM$  data symbols are transmitted in a GFDM block, which is given by

$$x[n] = \sum_{k=0}^{K-1} \sum_{m=0}^{M-1} d_{k,m} g[\langle n - mK \rangle_N] e^{j2\pi \frac{k}{K} n}, \quad (1)$$

where  $d_{k,m}$  is the data symbol carried by the  $k$ th sub-carrier at the  $m$ th sub-symbol,  $g[n]$  is the transmission prototype pulse,  $\langle \cdot \rangle_N$  represents the modulo  $N$  operator and  $n = 0, 1, \dots, N-1$ .

Notably, each data symbol is transmitted in a version of the prototype pulse that is circularly shifted in time and frequency. These pulses can be arranged in a modulation matrix, given by

$$\mathbf{A} = [\mathbf{g}_{0,0} \quad \mathbf{g}_{1,0} \cdots \mathbf{g}_{K-1,0} \quad \mathbf{g}_{0,1} \cdots \mathbf{g}_{K-1,M-1}], \quad (2)$$

where

$$\mathbf{g}_{k,m} = g[\langle n - mK \rangle_N] e^{j2\pi \frac{k}{K} n} \quad (3)$$

is a vector that contains the samples from the circular shifted versions of the prototype pulse. Thus, (1) can be rewritten using the matrix notation as

$$\mathbf{x} = \mathbf{A}\mathbf{d}, \quad (4)$$

where  $\mathbf{d} = (\mathbf{d}_0^T \cdots \mathbf{d}_{M-1}^T)^T$  and  $\mathbf{d}_m = (\mathbf{d}_{0,m} \cdots \mathbf{d}_{K-1,m})^T$ .

The GFDM signal can achieve a reduced OOB emission by virtue of the circular filtering and the characteristics of the transmission pulse. As the future mobile network will have to coexist with other legacy technologies without introducing interference, the low OOB emission is an important feature for 5G Physical Layer (5GPHY).

A time-reversal space-time coding (TR-STC) scheme is applied to the modulated signal, resulting in two correlated versions of the transmission signal irradiated towards the two receiver antennas installed several wave lengths away. This technique permits the receiver to explore the diversity gain from the multi-path channel, heightening the overall system performance. A CP and a CS are added to the transmission signals aiming to protect the symbols from the inter-symbol interference (ISI) introduced by dispersive channels. A time window can also be applied to symbols in order to smooth the abrupt transitions between GFDM blocks and improve the reduction of the OOB emissions.

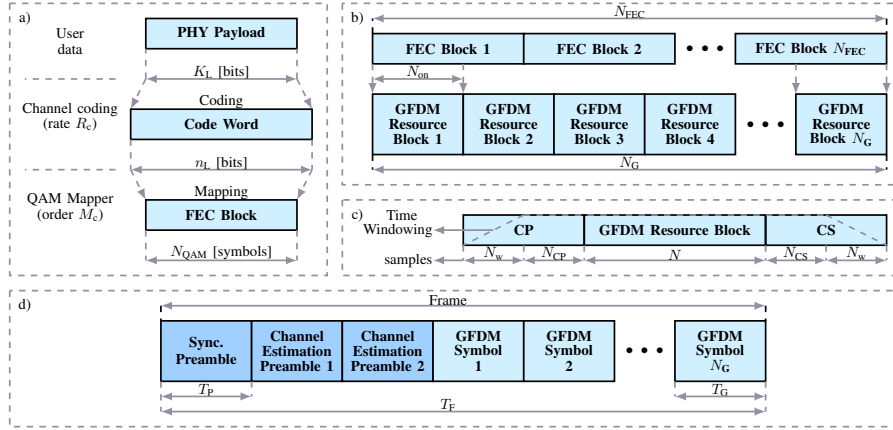


Fig. 2: Frame structure diagram [16].

The frame structure proposed for this transceiver is configurable and allows different operation modes in order to cover the requirements of the 5G scenarios. The frame formatter block multiplexes the user data with the synchronization and channel estimation preambles, used by the receiver to recover synchronism and perform the channel equalization. Figure 2 [16] details the frame structure. Most of transceiver parameters, such as coding rate, modulation order, number of active sub-carriers/sub-symbols and occupied bandwidth, CP/CS/Windowing length and the rate of synchronization/channel estimation preambles are allowed to be configured according with channel conditions and application requirements.

The transceiver implementation also comes with a digital pre-distortion (DPD) in order to reduce the effect of the non-linear distortions introduced by the high power amplifier (HPA) and consequently spectral regrowth, caused by the inherent high peak to average power ratio (PAPR) of multi-carrier systems, once the high amplitude peaks can lead the HPA to its non-linear region, resulting in high OOB emissions and inter-carrier interference (ICI).

At the receiver side, right after the RF front-end, the automatic gain control (AGC) block operates to normalize the input level and to properly exploit the dynamic range of the analogic-to-digital converter (ADC). The IQ balance block removes the in-phase and quadrature (IQ) imbalance introduced by the RF chain. Time and frequency synchronization is performed using the transmitted preamble and its locally stored replica, where frame structure timing is recovered and its portions are identified. Following synchronization, the channel frequency responses based on the received preambles are estimated. The channel frequency responses are then used by the space-time (ST) decoder to combine the received GFDM blocks from the multiple antennas, achieving a diversity gain. Since the transceiver employs two transmit and receive antennas, the system can achieve a diversity of order 4 (MIMO 2x2).

The ST decoder equalizes the combined signal and delivers it to the GFDM demodulator to recover the transmitted QAM sequence. The current version of the transceiver employs a zero-forcing demodulator, which uses an inverse of the

modulation matrix as follows

$$\hat{\mathbf{d}} = \mathbf{B} \mathbf{y}_{\text{eq}}, \quad (5)$$

where  $\mathbf{y}_{\text{eq}}$  is the equalized received signal at the output of the ST decoder and

$$\mathbf{B} = \mathbf{A}^{-1} \quad (6)$$

is the demodulation matrix.

The recovered QAM data feeds the symbol de-mapper block and the resulting bit sequence is used by the channel decoder block for correcting errors introduced by the channel. Then bit stuffing removal is applied in order to recover only the relevant transmitted information.

### III. PERFORMANCE ANALYSIS

The performance analysis presented in this paper is divided in two key performance indicators (KPIs). The first one is the system BER, while the second one is the OOB emissions.

#### A. BER performance analysis

A Monte Carlo process was conducted in order to obtain the overall system performance. The transmission channel is performed by a built-in channel simulator in the transceiver. As a reference for the acquired results, an approximation curve for the theoretical GFDM BER with zero-forcing (ZF) receiver under AWGN is employed and given by [10]

$$P_b \simeq \left[ \frac{2(L-1)}{\mu L} \text{erfc}(\Gamma) - \left( \frac{L-1}{\sqrt{\mu L}} \right)^2 \text{erfc}^2(\Gamma) \right], \quad (7)$$

where  $\text{erfc}(\cdot)$  is the complementary error function,  $L = \sqrt{M_c}$ , with  $M_c$  being the QAM constellation size,  $\mu = \log_2(M_c)$  and

$$\Gamma = \frac{3\eta \text{SNR}}{2(L^2 - 1)\xi} \quad (8)$$

with  $\eta$  representing the frame structure efficiency, considering the CP, CS and inserted preambles. The signal-to-noise ratio (SNR) is in linear scale and  $\xi = \sum_{n=0}^{N-1} |\gamma[n]|^2$  is the noise enhancement factor (NEF) due to the zero-forcing demodulation employed, with  $\gamma[n]$  being the samples of the prototype receiver pulse.

The waveform parameters used in the simulations and measurements are described in Table I. The demodulator used in the simulation is the ZF, the same implemented on the hardware prototype.

TABLE I: Waveform parameters used in simulation and measurements.

Parameter	Value
Constellation size	64-QAM
$K$	512
$M$	3
Prototype pulse	raised-cosine (RC) [10]
roll-off factor (ROF)	0.5
CP duration	32 samples
CS duration	16 samples
Window length	8 samples
Window type	4th RC [10]

Figure 3 shows the BER performance of the uncoded SISO GFDM in AWGN. The performance of the hardware prototype is shown assuming noiseless channel estimation and noisy channel estimation. It is possible to notice a degradation of approximately 2.5 dB at  $\text{BER} = 10^{-2}$  caused by the imperfect channel state information (CSI) used by the equalizer. However, the performance of the implemented hardware under noiseless channel estimation is close to the theoretical curve, showing that the impairments introduced by coefficient and samples quantizations and by the RF front-ends play a small role in the system performance. Figure 4 shows the BER

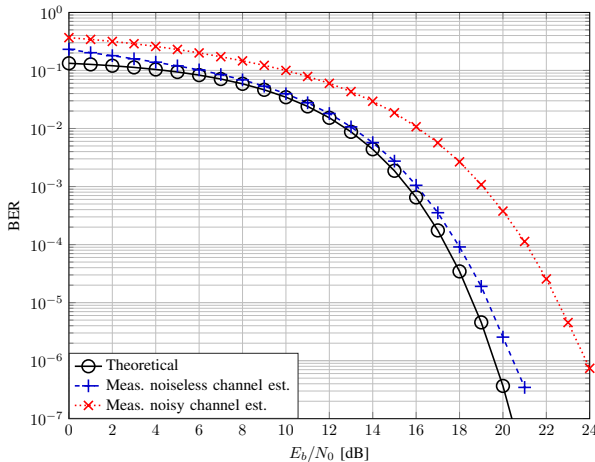


Fig. 3: Performance of the SISO GFDM transceiver operating with uncoded 64-QAM in AWGN channel.

performance of the uncoded MIMO GFDM in AWGN. As expected, the theoretical curve is 3 dB shifted from the SISO case, since half of the transmit power is employed by each transmit antenna [11]. The behavior of the prototype BER curves under noisy or noiseless channel estimation is the same as in the SISO case.

The polar code used in the evaluation of the prototype is described in Table II. A simulation comprising the waveform and polar code with the same parameters implemented in hardware was performed and the simulated BER curve is used as reference for the measured results.

Figure 5 shows the BER performance of the coded SISO GFDM under AWGN. The evaluation was also performed

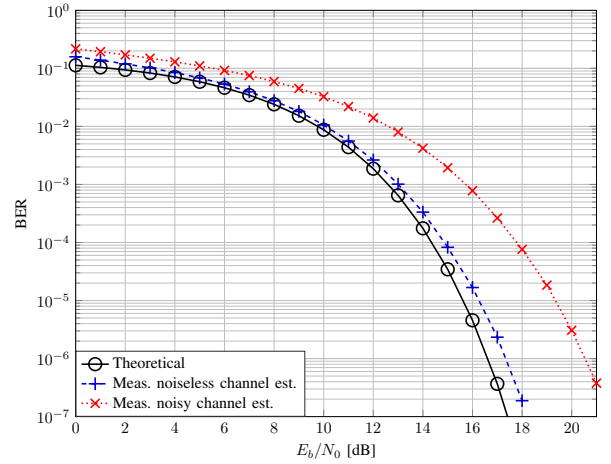


Fig. 4: Performance of the MIMO GFDM transceiver operating with uncoded 64-QAM in AWGN channel.

TABLE II: Polar code parameters

Parameter	Value
Code length (N)	2048
Shortened bits	32
Code rate	3/4
Decoded type	SCD

under noiseless and noisy channel estimations. Figure 6

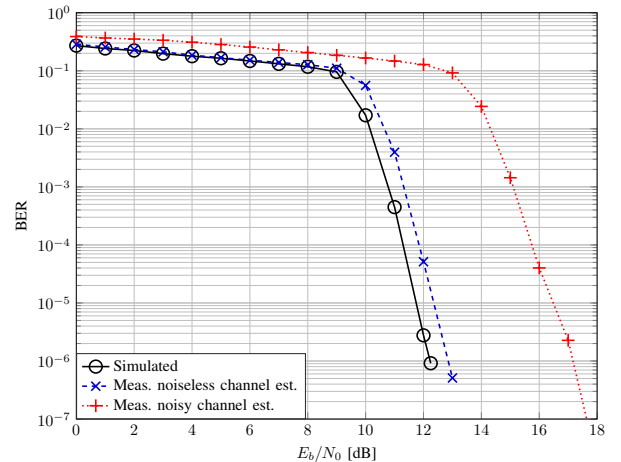


Fig. 5: Coded SISO-GFDM BER performance under AWGN channel.

shows the BER performance of the coded MIMO GFDM also under AWGN channel. For both, SISO and MIMO test cases, the noisy channel estimation caused a degradation of approximately 3.6 dB at  $\text{BER} = 10^{-6}$ . For noiseless channel estimation, the performance is within 1 dB from the simulated error rate. Again, the performance loss introduced by practical implementation issues can be considered satisfactory.

### B. OOB emissions analysis

OOB emission is an important KPI for remote areas applications because it is likely that CR technologies will be used to exploit TV white space (TVWS) and, therefore, to reduce cost [17]. Figure 7 compares the OOB emission from GFDM and OFDM signals.

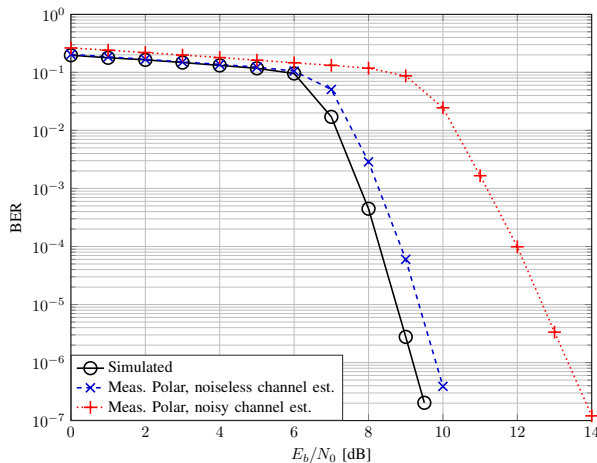


Fig. 6: Coded MIMO-GFDM BER performance under AWGN channel.

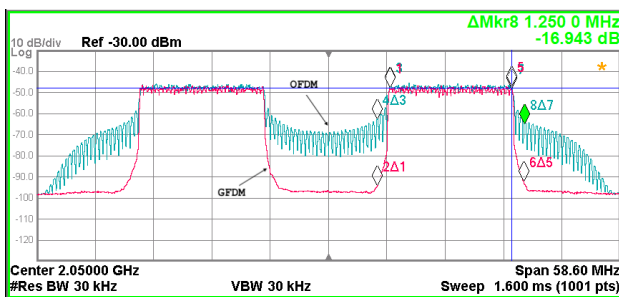


Fig. 7: GFDM and OFDM OOB emissions.

Both signals spans 36 MHz in total and the central 12 MHz portion are switched off. The OFDM signal presents very high OOB emissions, achieving  $-20$  dBc at the center of the unoccupied channel, which is almost 30 dB higher than the noise floor. These emissions can hinder the use of OFDM in applications where coexistence with other legacy technologies and spectrum mobility are required. GFDM, on the other hand, presents very low OOB emissions, achieving almost  $-50$  dBc at the center of the unoccupied channel. In fact, the GFDM OOB emissions cannot be distinguished from the measurement equipment error floor. GFDM can be used in TVWS scenarios where incumbents users must be protected against harmful interference.

#### IV. CONCLUSION

5G for remote area networks will face several challenges to provide reliable high throughput Internet access in low populated areas. Robustness for covering large distances and low OOB emissions are important KPIs to be achieved. This paper has shown that modern waveforms and channel codes can be used to reduce the undesired emissions and improve BER performance under AWGN channels. The coded and uncoded BER performance of the implemented transceiver, under noiseless channel estimation, is close to the theoretical curve. This result indicates that the digital signal processing chain, as well as the RF analog signal chain, play a small hole in the overall system performance. Conversely, the error rate

under noisy channel estimation suggests that there is room for improvement in the estimation process.

The measured OOB emissions confirm that GFDM has a very well confined spectrum, while OFDM spreads harmful interference when it is not filtered. Hence, the former is more suitable for remote areas applications than the later, since CR techniques is likely to be employed to allow for TVWS exploitation and fragmented spectrum allocation.

#### REFERENCES

- [1] M. Simsek, D. Zhang, D. Öhmann, M. Matthé, and G. Fettweis, "On the flexibility and autonomy of 5g wireless networks," *IEEE Access*, vol. 5, pp. 22 823–22 835, June 2017.
- [2] R. Vannithamby and S. Talwar, *Collaborative 5G Research within the EU Framework of Funded Research*. Wiley Telecom, 2017, pp. 472–.
- [3] L. Chiaraviglio *et al.*, "5g in rural and low-income areas: Are we ready?" in *2016 ITU Kaleidoscope: ICTs for a Sustainable World (ITU WT)*, Nov 2016, pp. 1–8.
- [4] V. Popescu, M. Fadda, and M. Murrone, "Performance analysis of ieee 802.22 wireless regional area network in the presence of digital video broadcasting: second generation terrestrial broadcasting services," *IET Communications*, vol. 10, no. 8, pp. 922–928, May 2016.
- [5] S. Sun and Z. Zhang, "Designing practical polar codes using simulation-based bit selection," *IEEE Journal on Emerging and Selected Topics in Circuits and Systems*, vol. 7, no. 4, pp. 594–603, Dec 2017.
- [6] H. Suzuki *et al.*, "Highly spectrally efficient ngara rural wireless broadband access demonstrator," in *2012 International Symposium on Communications and Information Technologies (ISCIT)*, Oct 2012, pp. 914–919.
- [7] Q. Y. Yu *et al.*, "Minimum sum-mean-square-error frequency-domain pre-coding for downlink multi-user mimo system in the frequency-selective fading channel," *IEEE Transactions on Wireless Communications*, vol. 16, no. 6, pp. 3573–3589, June 2017.
- [8] A. Markhasin, V. Belenky, V. Drozdova, A. Loshkarev, and I. Svinarev, "Cost-effective ubiquitous iot/m2m/h2h 5g communications for rural and remote areas," in *2016 International Conference on Information Science and Communications Technologies (ICISCT)*, Nov 2016, pp. 1–8.
- [9] L. Chiaraviglio, N. Blefari-Melazzi, W. Liu, J. A. Gutierrez, J. van de Beek, R. Birke, L. Chen, F. Idzikowski, D. Kilper, P. Monti, A. Bagula, and J. Wu, "Bringing 5g into rural and low-income areas: Is it feasible?" *IEEE Communications Standards Magazine*, vol. 1, no. 3, pp. 50–57, Sep 2017.
- [10] N. Michailow *et al.*, "Generalized Frequency Division Multiplexing for 5th Generation Cellular Networks," *IEEE Transactions on Communications*, vol. 62, no. 9, pp. 3045–3061, Sept 2014.
- [11] M. Matthé, L. L. Mendes, N. Michailow, D. Zhang, and G. Fettweis, "Widely linear estimation for space-time-coded gfdm in low-latency applications," *IEEE Transactions on Communications*, vol. 63, no. 11, pp. 4501–4509, Nov 2015.
- [12] M. Matthé, D. Zhang, and G. Fettweis, "Low-complexity iterative mmse-pic detection for mimo-gfdm," *IEEE Transactions on Communications*, vol. PP, no. 99, pp. 1–1, Dec 2017.
- [13] E. Sasoglu, *Polarization and Polar Codes*. Now Foundations and Trends, 2012. [Online]. Available: <http://ieeexplore.ieee.org/xpl/articleDetails.jsp?arnumber=8187298>
- [14] A. Sharma and M. Salim, "Polar code: The channel code contender for 5g scenarios," in *2017 International Conference on Computer, Communications and Electronics (Comptelix)*, July 2017, pp. 676–682.
- [15] R. Wang and R. Liu, "A novel puncturing scheme for polar codes," *IEEE Communications Letters*, vol. 18, no. 12, pp. 2081–2084, 2014.
- [16] J. S. Ferreira *et al.*, "GFDM Frame Design for 5G Application Scenarios," *Journal of Communication and Information Systems*, vol. 32, no. 1, 2017.
- [17] P. Steenkiste, D. Sicker, G. Minden, and D. Raychaudhuri, "Future directions in cognitive radio network research," NSF Workshop Report, Tech. Rep., 2009.